Stem Cell Reports
Article

ISSCR

OPEN ACCESS

Human iPSC-based neurodevelopmental models of globoid cell leukodystrophy uncover patient- and cell type-specific disease phenotypes

Elisabeth Mangiameli,[1] Anna Cecchele,[1] Francesco Morena,[2] Francesca Sanvito,[3] Vittoria Matafora,[4] Angela Cattaneo,[4] Lucrezia della Volpe,[1] Daniela Gnani,[1] Marianna Paulis,[5,6] Lucia Susani,[5,6] Sabata Martino,[2] Raffaella Di Micco,[1] Angela Bachi,[4] and Angela Gritti[1,*]

[1]San Raffaele Telethon Institute for Gene Therapy (SR-Tiget), IRCCS San Raffaele Scientific Institute, Via Olgettina 60, 20132 Milan, Italy
[2]Department of Chemistry, Biology and Biotechnology, University of Perugia, Via del Giochetto, 06123 Perugia, Italy
[3]Pathology Unit, IRCCS San Raffaele Scientific Institute, Via Olgettina 60, 20132 Milan, Italy
[4]IFOM-FIRC Institute of Molecular Oncology, Via Adamello 16, 20139 Milan, Italy
[5]Humanitas Clinical and Research Center-IRCCS, Rozzano, Milan, Italy
[6]National Research Council (CNR)-IRGB/UOS of Milan, Milan, Italy
*Correspondence: gritti.angela@hsr.it
https://doi.org/10.1016/j.stemcr.2021.04.011

SUMMARY

Globoid cell leukodystrophy (GLD) is a rare neurodegenerative lysosomal storage disease caused by an inherited deficiency of β-galactocerebrosidase (GALC). GLD pathogenesis and therapeutic correction have been poorly studied in patient neural cells. Here, we investigated the impact of GALC deficiency and lentiviral vector-mediated GALC rescue/overexpression in induced pluripotent stem cell (iPSC)-derived neural progenitors and neuronal/glial progeny obtained from two GLD patients. GLD neural progeny displayed progressive psychosine storage, oligodendroglial and neuronal defects, unbalanced lipid composition, and early activation of cellular senescence, depending on the disease-causing mutation. The partial rescue of the neural differentiation program upon GALC reconstitution and psychosine clearance suggests multiple mechanisms contributing to neural pathology in GLD. Also, the pathological phenotype associated to supraphysiological GALC levels highlights the need of regulated GALC expression for proper human neural commitment/differentiation. These data have important implications for establishing safe therapeutic strategies to enhance disease correction of GLD.

INTRODUCTION

Globoid cell leukodystrophy (GLD, or Krabbe disease) is a rare lysosomal storage disorder (LSD) due to an inherited deficiency of β-galactocerebrosidase (GALC), a catabolic enzyme of galactosphingolipids, e.g., galactosylceramide and galactosylsphingosine (psychosine) (Suzuki and Suzuki, 1970). The infantile forms present with relentless demyelination and neurodegeneration of the central nervous system (CNS) and peripheral nervous system. Allogeneic hematopoietic stem/progenitor cell (HSPC) transplant partially corrects the CNS pathology (Allewelt et al., 2016), likely because of the modest GALC supply provided by HSPC myeloid progeny in the brain. *In vivo* and *ex vivo* gene therapy (GT) using lentiviral vectors (LVs) and adeno-associated vectors benefit GLD animal models (Bradbury et al., 2021; Ricca and Gritti, 2016). Still, the obstacles in reaching safe, widespread, and stable expression of therapeutic GALC levels in the CNS currently limit the clinical application of GT strategies.

Besides acting on myelin and axons, psychosine and related substrates affect glial and neuronal cell homeostasis interfering with lipid content/distribution (White et al., 2011), altering proteostasis (Pellegrini et al., 2019) and autophagy (Del Grosso et al., 2019), promoting apoptosis (Jatana et al., 2002) and lysosomal dysfunction (Folts et al., 2016). Growing evidence points to a previous underestimated association between lysosomal dysfunction, protein misfolding/aggregation, lipid unbalance, and senescence in multiple organisms and cell types (Irahara-Miyana et al., 2018; Lizardo et al., 2017; Trayssac et al., 2018). Also, recent observations implicate senescence of neural progenitors (NPCs) and oligodendroglial progenitors in the pathogenesis of neurodegenerative disorders with protein aggregation (Zhang et al., 2019) and neuroinflammatory demyelinating disorders (Nicaise et al., 2019), providing a strong rationale for investigating these processes as potential contributors to GLD pathology.

The GALC precursor protein (80 kDa) is glycosylated in the Golgi apparatus and is activated in the lysosomes by cleavage and assembling of the 50 and 30 kDa forms into the active multimeric enzyme. The fraction of precursor protein escaping the physiological lysosomal targeting is secreted and available for cross-correction of neighboring cells, a mechanism at the basis of enzyme replacement therapies. More than 200 pathogenic variants have been identified in the human *GALC* gene, among which a 30 kb deletion accounts for 45% of pathogenic alleles in individuals of European origin (Orsini et al., 2000). The occurrence of this gene deletion in the homozygous state or compound heterozygous state with another severe pathogenic variant results in the infantile-onset forms of GLD. The genotype-phenotype correlation is less clear for the many missense/nonsense mutations occurring in homozygosis or compound heterozygosis, which may be associated with variable residual

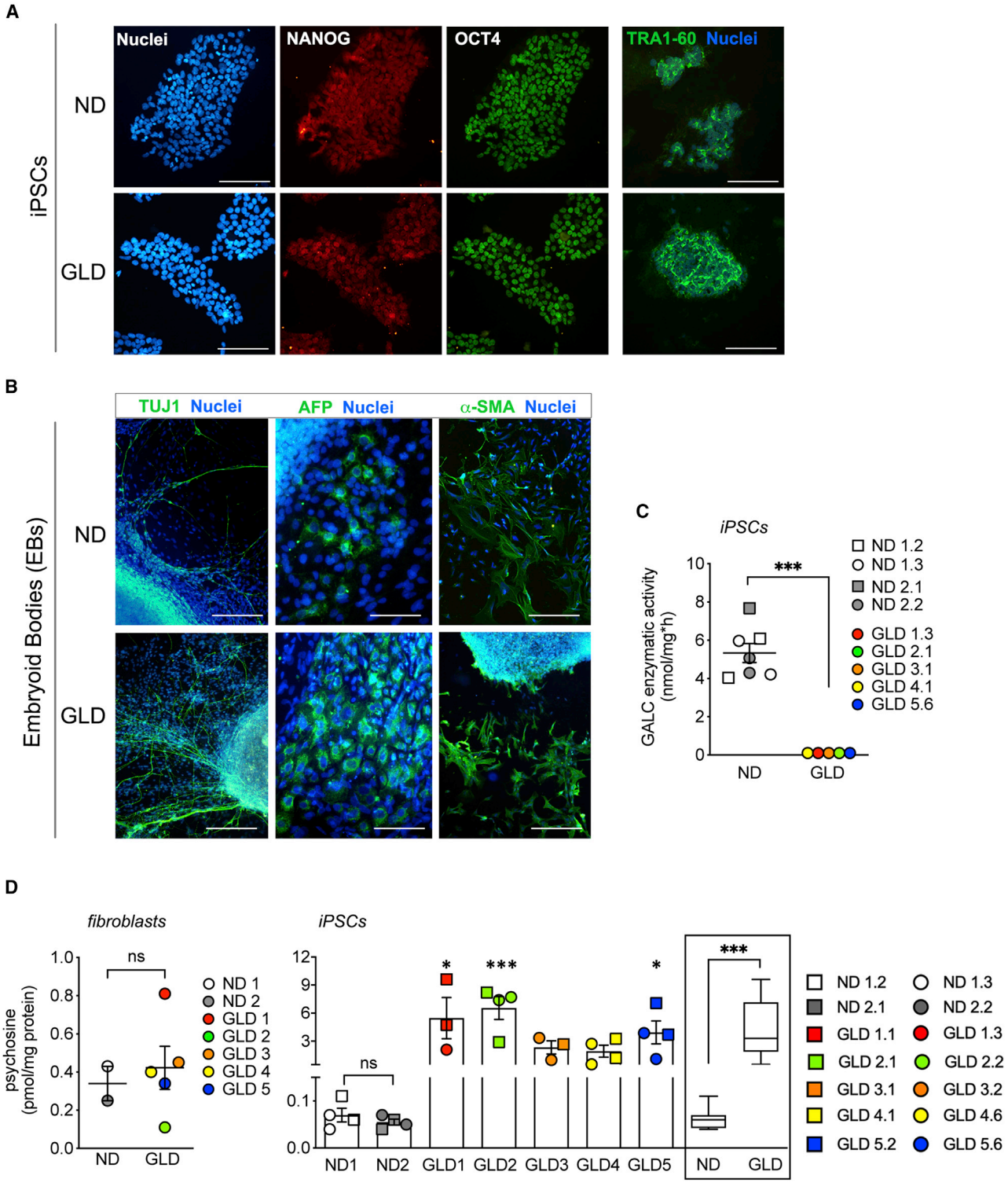

Figure 1. GLD iPSCs have undetectable GALC activity and increased psychosine levels

(A) Immunofluorescence pictures of ND and GLD iPSCs expressing OCT4 (green), NANOG (red), and TRA 1-60 (green). Nuclei counterstained with Hoechst (blue). Scale bars, 100 μm.

(B) Immunofluorescence pictures showing cells expressing AFP, α-SMA, and TUJ1 (green) in ND and GLD embryoid bodies (EBs). Nuclei counterstained with Hoechst (blue). Scale bars, 80 μm (AFP), 200 μm (TUJ1, α-SMA).

(legend continued on next page)

GALC activity and severe to mild disease variants (De Gasperi et al., 1999; Jalal et al., 2012). Misfolded GALC proteins evoke an unfolded protein response activation (Irahara-Miyana et al., 2018) and show mutation-specific alteration of lysosomal trafficking and processing (Shin et al., 2016), pointing to pathological cascades that are independent of, or act in synergy with, the primary storage.

Small and large GLD animal models (Wenger, 2000) have been widely used to study primary and secondary pathological events and to test novel therapies. Still, most of them carry spontaneous mutations that are not found in humans and partially recapitulate the spectrum of pathological manifestations observed in patients. GLD human cellular models include patient-specific fibroblasts (Ribbens et al., 2013; Spratley et al., 2016), hematopoietic cells (Martino et al., 2009), or epithelial cell lines with induced GALC mutations (Lee et al., 2010; Shin et al., 2016) that hardly recapitulate the metabolic and functional features of neural cells. Human induced pluripotent stem cells (iPSCs) (Yamanaka, 2007) offer a unique tool to analyze disease pathogenesis in a patient-specific genetic background and to test correction strategies. The differentiation of iPSCs in neural cells has boosted CNS disease modeling and therapeutic screening (Shi et al., 2017). Human iPSCs are available from a variety of LSDs (Huang et al., 2012) but no reports are describing GLD iPSCs.

Here, we established GLD patient-specific iPSC lines as a reliable human model for elucidating GLD pathogenesis and testing the efficacy of GT in relevant neural cell types. To this end, we differentiated GLD iPSCs into neural progenitor cells (NPCs) and differentiated progeny (oligodendrocytes, neurons, and astrocytes) and monitored the progression of cell-type- and patient-specific primary and secondary defects. Finally, we assessed the impact of GALC reconstitution/overexpression (achieved by LV-mediated gene transfer) in reverting the pathological phenotype and its potential effect on the biology of human NPCs and progeny.

RESULTS

GLD iPSCs show undetectable GALC activity and psychosine storage but display normal pluripotency features

We generated iPSCs from fibroblasts of five GLD infantile patients with distinct biallelic mutations in the *GALC* gene. Control iPSC lines were generated from fibroblasts of two unrelated normal donors (ND1, adult; ND2, neonatal) and one non-affected relative (ND3) (Table S1). GALC activity in fibroblasts was 2.42 nmol·h/mg (ND1), 3.89 nmol·h/mg (ND2), and 1.56 nmol·h/mg (ND3), while it was undetectable in all GLD cells. By using an integration- and feeder-free system we obtained several iPSC clones from each GLD and ND fibroblast line (reprogramming efficiency: 2%–53%) (Figure S1A). After six to ten subculturing passages, we randomly selected two clones/line for further analysis (Figure S1A). The presence of *GALC* mutations was verified by PCR analysis and sequencing (Figures S1B and S1C).

We assessed the expression of the pluripotency markers NANOG, SOX2, KLF4, OCT4, and TRA1-60 in GLD and ND iPSC clones by RT-PCR (Figure S1D) and immunofluorescence (IF) (Figure 1A). Analysis of endodermal-, mesodermal-, and ectodermal-specific markers in embryoid bodies (Figures 1B and S1E) and histological assessment of teratomas (Figure S1F) confirmed the pluripotency of GLD and ND iPSCs.

GLD iPSC clones displayed undetectable GALC activity (Figure 1C) and significant psychosine storage (50- to 100-fold the ND levels) that was absent in parental fibroblasts (Figure 1D).

Overall, GLD patient iPSCs showed the primary biochemical GLD hallmarks while retaining normal stem cell properties, justifying their use as a human-based GLD model.

LV-mediated gene transfer in GLD iPSCs rescues GALC activity and normalizes psychosine storage

We selected GLD1 and GLD5 lines (two clones/line) for further characterization and gene transfer studies. GLD1 is homozygous for the large 30 kb *GALC* gene deletion that produces a truncated protein lacking the whole coding region for the 30 kDa subunit and 15% of the coding region for the 50 kDa subunit (Luzi et al., 1995). GLD5 is homozygous for a missense mutation (c.1657G > A) that is predicted to cause protein misfolding (De Gasperi et al., 1999). ND1 and ND2 iPSCs (two clones/line) were used as controls (Table S1; Figure S1A). We selected iPSCs with normal karyotype (Figure S1G; Table S2) and used these cells within subculturing passages 8–30.

To restore GALC activity, we transduced GLD1 and GLD5 iPSC clones with a VSV-pseudotyped third-generation LV

(C) GALC enzymatic activity (mean ± SEM) in ND and GLD iPSC clones; Mann-Whitney test; ***p < 0.001.
(D) Psychosine levels (mean ± SEM) in ND1 (white circles), ND2 (gray circles), and GLD (colored circles) fibroblasts (n = 1 sample/line) and corresponding iPSCs (n = 2 clones/line, in single or duplicate). Mann-Whitney test (fibroblasts) and Kruskal-Wallis test followed by Dunn's multiple comparison test (iPSCs); ns, not significant; *p < 0.05, ***p < 0.001 versus ND (mean). The mean ± SEM of all ND and GLD clones is plotted in the box and whiskers graph and analyzed by Mann-Whitney test; ***p < 0.001.
See also Figure S1.

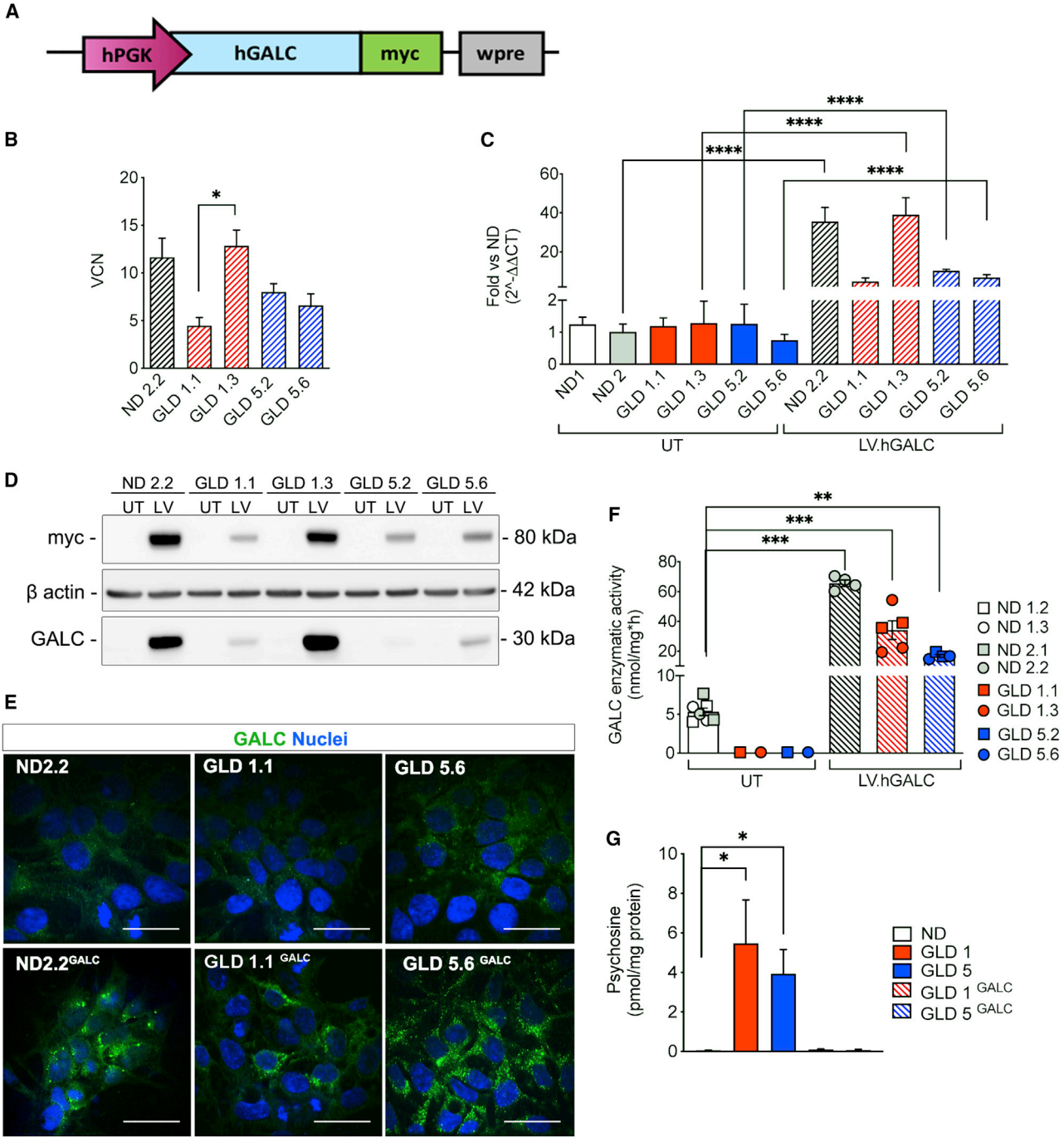

Figure 2. LV-mediated gene transfer rescues GALC expression and enzymatic activity in GLD iPSCs

(A) Schematic representation of the LV.hGALC vector. hPGK, human phosphoglycerate kinase promoter; wpre, woodchuck hepatitis virus post-transcriptional regulatory element.

(B) Vector copy number (mean ± SEM) measured in ND and GLD iPSCs clones transduced with LV.hGALC (MOI2). n = 2–4 independent experiments/clone; Kruskal-Wallis test followed by Dunns' multiple comparison post-test; *p < 0.05.

(C) GALC mRNA expression (mean ± SEM) in untransduced (UT); (solid bars) and LV.hGALC-transduced (striped bars). n = 3 independent experiments/clone. Values are normalized on GAPDH and expressed as fold change (2^-ΔΔCT) versus ND (mean); one-way ANOVA followed by Tukey's multiple comparison post-test; ****p < 0.0001.

(legend continued on next page)

encoding for the human (h) *GALC* gene tagged with the Myc peptide (LV.hGALC) (Meneghini et al., 2016) (Figure 2A). We transduced GLD1.1, GLD1.3, GLD5.2, GLD5.6, and ND2.2 iPSC clones using LV.hGALC at multiplicity of infection (MOI) of 2 based on pilot dose-response experiments (Figure S2A). LV.hGALC-transduced GLD (GLD^{GALC}) and ND (ND^{GALC}) iPSCs showed vector copy number (VCN) ranging from 5 to 15 (Figure 2B) and significant GALC mRNA (Figure 2C) and protein expression by western blot (WB) (Figure 2D; the anti-myc and the anti-GALC antibodies recognize the 80 kDa precursor protein and the 30 kDa cleaved fragment, respectively) and IF analysis (Figure 2E; the antibody recognizes the full-length protein). We documented a correlation between VCN, GALC mRNA expression, and enzymatic activity (Figure S2B), which reached supraphysiological levels (Figure 2F).

The transgenic GALC enzyme normalized psychosine levels in GLD iPSCs (Figure 2G), which do not show GalCer accumulation or increased expression of the lysosomal protein LAMP1 (index of lysosomal expansion) (Figures S2C and S2D). Importantly, LV transduction and GALC overexpression did not affect the pluripotency (Figure S2E) and proliferation (Figure S2F) of ND and GLD iPSC clones.

GLD and ND iPSC-derived NPCs are generated with similar efficiency and show a comparable phenotype

We next assessed the impact of GALC deficiency and LV-mediated GALC rescue in iPSC-derived neural cells. We differentiated ND, GLD, GLD^{GALC}, and ND^{GALC} iPSCs into NPCs by applying a published protocol (Chambers et al., 2009) (Figure 3A). NPCs showed downregulation of pluripotency markers (*OCT4*, *NANOG*) and upregulation of NPC markers (*NESTIN*, *PAX6*, *FOXG1*) as well as early neuronal (doublecortin [*DCX*]) and glial cell (*ASCL1*) markers (Figures 3B and 3C). We obtained NPCs with similar efficiency from untransduced (UT) and LV.hGALC-transduced GLD and ND iPSCs with the only exception of clone $GLD1.3^{GALC}$, which consistently displayed modest *PAX6* upregulation and Nestin expression (Figures 3B and S3) and was excluded from further analysis. The selected NPC lines were composed of 90%–100% of PAX6+ and Nestin+ cells (Figure S3) and were expanded in culture for five to six passages in the presence of neural medium (Figure 3D). Thus, ND and GLD iPSC-derived NPCs display bona-fide NPC molecular and phenotypic features.

Time- and cell-type-dependent transcriptional regulation of GALC expression and activity during differentiation of NPCs into neurons and glia

We adapted a published protocol (Frati et al., 2018) to generate mixed cell populations containing neurons, astrocytes, and oligodendrocytes from ND, GLD, GLD^{GALC}, and ND^{GALC} NPCs. Cultures were evaluated at day 0 (d0; NPCs), d7, d14, and d24 of differentiation (Figure 3E), to monitor GALC expression/activity and glial/neuronal cell commitment and maturation by means of biochemical and molecular analysis.

The GALC transcript was expressed at low levels in ND and GLD iPSC clones (GLD1 and GLD5 mutations are not predicted to impact mRNA transcription) and was upregulated upon neural differentiation (Figure 3F). GALC mRNA expression in GLD^{GALC} and ND^{GALC} iPSCs was constant over time, due to the high and stable expression driven by the constitutive phosphoglycerate kinase (PGK) promoter (Figure 3F).

ND NPCs and differentiated cultures (d14 and d24) showed comparable GALC enzymatic activity (Figure 3G). The supraphysiological ($\approx$10× the normal levels) GALC activity in GLD^{GALC} iPSCs decreased during the neural differentiation to reach physiological levels at d14 and d24, whereas ND^{GALC} cultures maintained supraphysiological GALC activity ($\approx$3-fold the ND counterpart at d14 and d24) (Figure 3G). The stable VCN measured in ND^{GALC} and GLD^{GALC} cultures at different time points of differentiation (Figure 3H) suggested that decreased enzymatic activity is not resulting from the counter selection of cells harboring high VCN.

Overall, these data show that LV-mediated gene transfer ensures (supra)physiological GALC expression and activity in NPCs and neuronal/glial progeny, and highlight a stringent transcriptional regulation of GALC activity during iPSC to neural differentiation.

(D) Western blot showing the expression of the GALC-myc fusion protein using an anti-myc antibody (recognizing the 80 kDa precursor protein) and an anti-hGALC antibody (recognizing the 30 kDa cleaved protein) in LV.hGALC-transduced (LV; MOI2), ND, and UT GLD iPSC clones. β-Actin, loading control. UT clones do not express the myc-tagged protein. The 30 kDa band is undetectable in UT clones due to the low physiological GALC expression.

(E) Immunofluorescence pictures showing the expression of the GALC protein (green; anti-hGALC) in UT and LV.hGALC transduced ND and GLD iPSCs. Nuclei counterstained with Hoechst (blue). Scale bars, 20 μm.

(F and G) GALC enzymatic activity (F) and psychosine levels (G); clones as in (F) in UT (solid bars) and LV.hGALC transduced (striped bars) ND, GLD, and iPSCs. Data are the mean ± SEM (n = 2–4 independent experiments/clone). Kruskal-Wallis test followed by Dunn's multiple comparison post-test (ND selected as control group); *p < 0.05, **p < 0.01, ***p < 0.001; ns, not significant.

See also Figure S2.

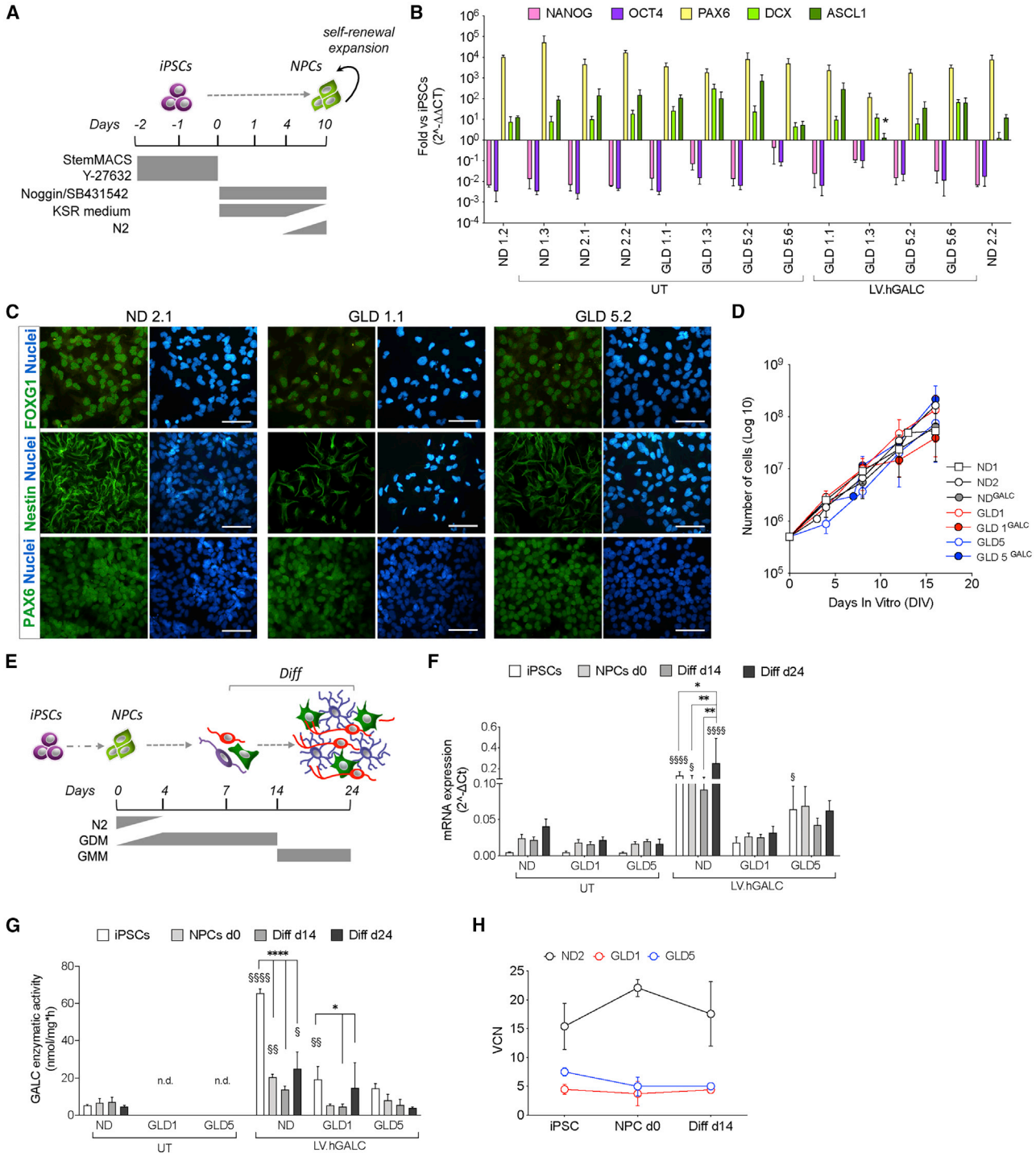

Figure 3. Differentiation of ND and GLD iPSCs into NPCs, neurons, and glial cells

(A) Protocol used to differentiate iPSCs into NPCs. KSR, knockout serum replacement; N2, neural medium. GDM, glial differentiation medium; GMM, glial maturation medium.

(B) Expression of NANOG, OCT4, PAX6, DCX, and ASCL1 in untransduced (UT) and LV.hGALC-transduced ND and GLD NPC populations (SYBR green RT-PCR). Data are normalized on GAPDH expression and shown as fold change (2^-ΔΔCT) on the corresponding iPSC clone. Data are the mean ± SEM (n = 3–4 independent experiments/clone). The GLD1.3^{GALC} clone shows reduced PAX6 upregulation. Kruskal-Wallis test followed by Dunn's multiple comparison post-test (ND, control group). *p < 0.05.

(legend continued on next page)

GLD NPCs display defective neural and glial differentiation: Impact of GALC rescue/overexpression on psychosine levels and phenotype

To study the impact of GALC mutations on the glial and neuronal differentiation program and the effect of LV-mediated GALC restoration, we performed a comprehensive molecular, biochemical, and phenotypic analysis on ND and GLD NPCs and neuronal/glial progeny.

The expression pattern of the master oligodendroglial gene *OLIG2* observed in GLD1 and GLD5 cells suggested an altered oligodendroglial differentiation program, which was partially normalized in GLD^{GALC} cultures (Figure S4A). A similar or more severe alteration was observed in ND^{GALC} cultures, in which *OLIG2* expression was overall strongly reduced (Figure S4A). We detected an early and persistent reduction of OLIG2+ and APC+ cells (IF; Figures 4A–4C) and a significant downregulation of OLIG1 protein expression (WB; Figure S4B) in GLD1 and GLD5 cultures as compared with ND counterparts, highlighting a partial rescue in GLD^{GALC} cells and a detrimental impact of GALC overexpression in ND cultures (Figures 4A–4C and S4B).

The expression of the immature neuronal marker *DCX* was reduced in GLD5 (but not in GLD1) as compared with ND cells (Figure S4C). GLD5 cultures showed a significant time-dependent reduction of TUJ1+ neurons (Figures 4D and 4E), a decreased and/or delayed TUJ1 and neurofilament (NF)-M protein expression (Figures S4D and S4E), and a reduced expression of acetylated and polyglutamated tubulin and phosphorylated NF (d14 and d24; Figure S5). Overall, these data suggested neuronal loss and/or defective neuronal differentiation/maturation. In contrast, GLD1 cultures had normal proportions of neuronal cells (Figures 4D and 4E) and expression of neuronal proteins (Figures S4D and S4E). The neuronal defects were rescued in GLD5^{GALC} cultures (Figures 4D, 4E, S4D, and S4E). GLD^{GALC} cultures also showed an early upregulation of NF-M protein as compared with the UT ND counterparts (Figure S4E), suggesting an accelerated neuronal differentiation. GALC overexpression negatively affected the pattern of gene and protein expression (Figures S4 and S5), as well as the number and morphology of ND neurons (Figures 4D and 4E).

Astroglia is the less represented and most variable cell population in both ND and GLD differentiated cultures, with no clear differences related to GALC deficiency, as shown by glial fibrillary acidic protein (*GFAP*) gene expression analysis (Figure S5D), WB (Figure S5E), and IF (Figures 4D, 4F, and S5F; 3%–15% of GFAP+ cells on the total cells at d24).

Interestingly, both GALC deficiency (GLD cultures) and forced GALC expression (GLD^{GALC} and ND^{GALC} cultures) were associated to higher percentages of cells that stained negative for the selected lineage-specific markers (Figure S5F).

Psychosine levels were low in GLD NPCs and increased during differentiation up to ≈8 (GLD1) and ≈30-fold (GLD5) the ND levels at d24 (Figure 5A). The psychosine build-up was not associated with a significant increase of apoptotic cells (Figure 5B) or with enhanced phospholipase A2 (PLA2) activity (Figure 5C), which has been associated with psychosine-induced apoptosis (Misslin et al., 2017). Psychosine levels were normalized in GLD1^{GALC} cultures and strongly reduced in GLD5^{GALC} cultures (≈2-fold the ND levels), in line with the enzymatic reconstitution. We observed a moderate increase of Lysotracker+ area (Figure 5D) in GLD5 and, more evident, in GLD1 NPCs (normalized in GLD1^{GALC} cultures). Confocal IF analysis

(C) Immunofluorescence pictures showing the expression of Nestin, FOXG1, and PAX6 (green) in ND2.1, GLD1.2, and GLD5.2 NPCs cultures. Nuclei counterstained with DAPI (blue). Scale bars, 50 μm.

(D) Proliferation of UT and LV.hGALC-transduced ND and GLD NPC lines (subculturing passages 0 to 5; days *in vitro* [DIV]). Data are the mean ± SEM; n = 2–3 independent experiments, 1–2 clones/group. Clones used: ND1.2, ND1.3, ND2.1, ND2.2, GLD1.1, GLD1.3, GLD5.2, GLD5.6, ND2.2^{GALC}, GLD1.1^{GALC}, GLD5.2^{GALC}, and GLD5.6^{GALC}.

(E) Protocol used to differentiate NPCs (d0) into mixed neuronal/glial cultures that were analyzed at day 7 (d7), d14, and d24. GDM, glial differentiation medium; GMM, glial maturation medium.

(F) GALC mRNA expression (mean ± SEM) in UT and LV.hGALC-transduced iPSCs and neural progeny (NPCs, d0; differentiated cells, d14 and d24). Values are normalized on GAPDH and expressed as ($2^{-}\Delta CT$). Clones used: ND1.2, ND1.3, ND2.1, ND2.2, GLD1.1, GLD1.3, GLD5.2, GLD5.6, ND2.2^{GALC}, GLD1.1^{GALC}, GLD5.2^{GALC}, and GLD5.6^{GALC}. n = 2–3 independent experiments; 1–4 clones/group. Data analyzed using two-way ANOVA followed by (1) Tukey's multiple comparison post-test to compare the different time points in each group. *p < 0.05, **p < 0.01, ****p < 0.0001; (2) Dunnett's multiple comparison post-test to compare the different groups at each time point against ND (control group). §p < 0.05, §§p < 0.01, §§§§p < 0.0001.

(G) GALC enzymatic activity (mean ± SEM) in UT and LV.hGALC-transduced ND and GLD iPSCs and neural progeny (NPCs, d0; differentiated cells, d14 and d24). n = 2–4 independent experiments/clone. Kruskal-Wallis test followed by Dunn's multiple comparison post-test (ND, control group); *p < 0.01, ****p < 0.0001, §p < 0.05, §§p < 0.01, §§§§p < 0.0001; n.d., not detectable.

(H) Vector copy number (VCN) measured in LV.hGALC-transduced iPSCs, NPCs (d0) and differentiated cells (d14). Clones used: ND2.2^{GALC}, GLD1.1^{GALC}, GLD5.2^{GALC}, and GLD5.6^{GALC}; n = 1–3 independent experiments/clone, 1–2 clones/group.

See also Figure S3.

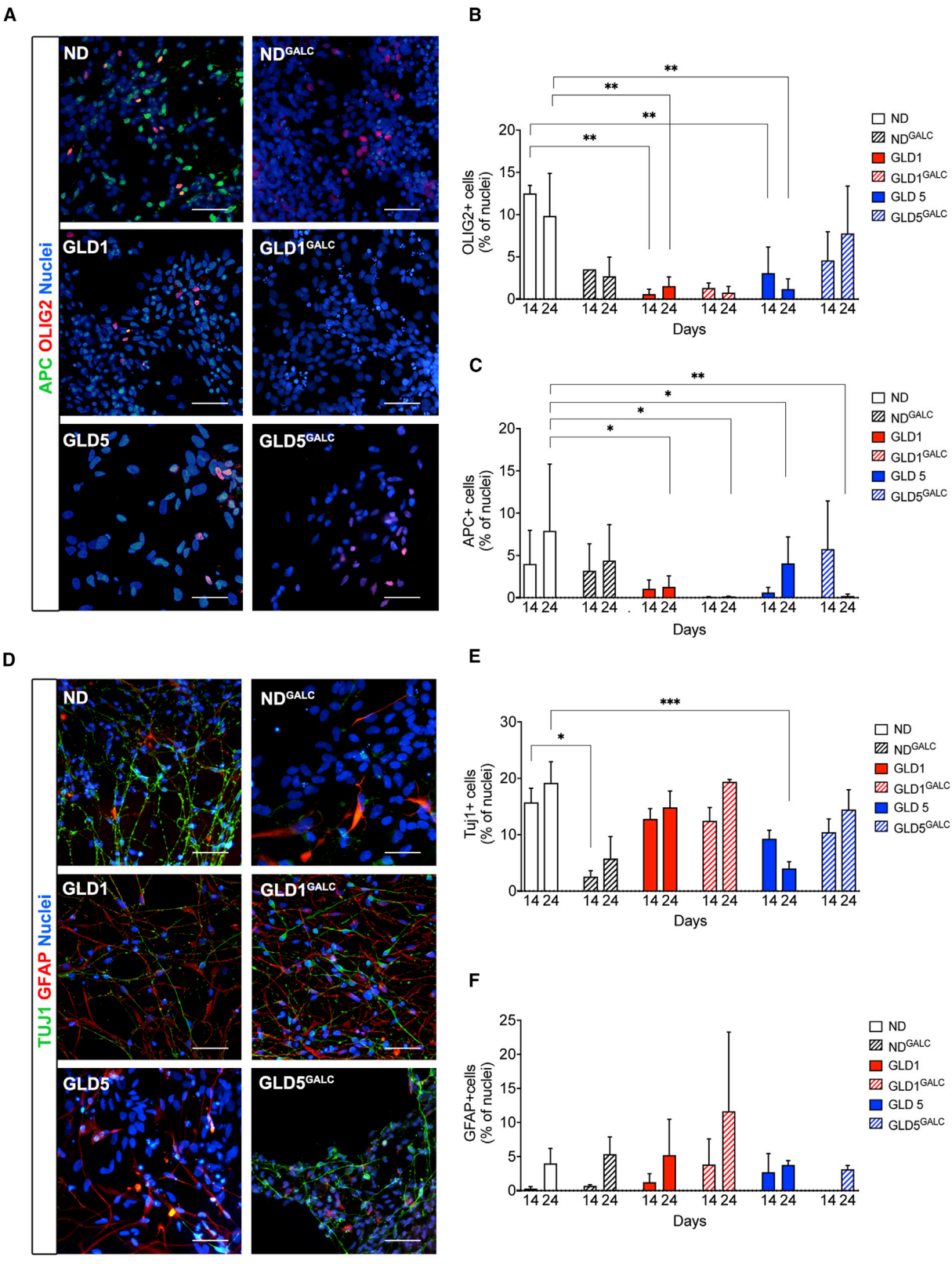

(legend on next page)

highlighted the presence of large LAMP1+ vesicles in GLD5 cells (occasionally in GLD1 cells) at d0 (Figure 5E) and d14 of differentiation (Figure 5F). This phenotype was partially normalized in GLD5^{GALC} cultures (Figures 5E and 5F). LAMP1 protein expression was comparable in ND, GLD, and GLD^{GALC} differentiated cultures, while it was increased in GALC-overexpressing ND cells (Figure 5G).

These data show that: (1) GALC deficiency impairs the neuronal and oligodendroglial differentiation of human NPCs, with cell-type- and patient-specific phenotypes; (2) LV-mediated GALC rescue reduces psychosine levels and partially rescues the GLD phenotype; (3) a tight regulation of GALC expression is required to ensure proper NPCs functionality and preserve multipotency.

Early activation of a senescence response in GLD5 iPSC-derived neural cells

Our data suggested a marginal contribution of cell death to the loss of GLD neurons and glial cells. Therefore, we explored whether the altered differentiation programs of GLD NPCs could be due to an altered proliferative potential. By performing and quantifying Ki67/Nestin immunostaining at different stages of the differentiation protocol, we showed a time-dependent decrease in the percentage of proliferating cells in all ND and GLD cultures, indicating the exit from the cell cycle of NPCs and acquisition of a post-mitotic state (Figures 6A and 6B). Interestingly, 5-ethynyl-2′-deoxyuridine (EdU) incorporation assay showed an earlier and more drastic drop in the percentage of cells in active S-phase in GLD5 cultures as compared with ND and GLD1 counterparts (Figure 6C). This proliferation drop was recovered in GLD5^{GALC} cultures (Figure 6C).

We next investigated whether the early proliferation arrest highlighted in GLD5 cultures was associated with the establishment of cellular senescence, a biological process characterized by growth arrest, accumulation of DNA damage, and activation of a pro-inflammatory program known as senescence-associated secretory phenotype (SASP) (He and Sharpless, 2017). We detected upregulation of the cell-cycle inhibitors p16 (Figure 6D) and p21 (Figures 6E and 6F) and increased nuclear levels of DNA damage response (DDR) markers 53BP1 (Figures 6G and 6H) and γH2AX (Figures S6A and S6B) as early as d7 post-differentiation. The induction of DDR and p21 protein was specific to GLD5 cultures, not reported in ND or GLD1 cultures, and partially rescued in GLD5^{GALC} cultures. We also observed a dramatic increase in the percentage of senescence-associated (SA)-β-GAL+ cells in GLD5 (but not ND or GLD1 cultures) with a peak at d7 of differentiation (Figures 6I and 6J) and induction of the SASP pro-inflammatory factors interleukin 6 (IL-6), IL-8, tumor necrosis factor alpha, and IL-1β (Figures S6C–S6F). Finally, consistent with the acquisition of a senescence phenotype, GLD5 cells displayed increased cell size/complexity (based on forward and side scatter parameters) and expanded nuclear area at d7 and d14 post-differentiation as compared with ND and GLD1 cells (Figures S6G–S6H). Importantly, these senescence-associated hallmarks were reduced or normalized in GLD5^{GALC} cultures.

Altogether, our data suggest that GLD5 iPSC-derived NPCs activate an early senescence program that hampers physiological lineage commitment/differentiation. This senescent phenotype is patient-specific (as it is not evident in GLD1 cells), and is rescued by supplying physiological levels of a functional GALC enzyme.

GLD cells display an altered lipidomic profile during the iPSC to neural differentiation

The GALC enzyme has a central role in the sphingolipid metabolism and sphingolipids have prominent activities in the CNS, inducing biological effects on various stem/progenitor cell types (Hannun and Obeid, 2017). To elucidate the impact of GALC absence/enhanced expression on the lipidome of iPSCs and neural progeny we performed an untargeted global lipidomic profiling in ND, GLD, and GLD^{GALC} iPSCs, NPCs, and neuronal/glial cells at d14 of differentiation.

We identified more than 800 lipid species, with a distinct signature and enrichment of specific lipid classes in iPSCs (e.g., triacylglycerols [TAGs]; lysophosphatidylserine), NPCs (e.g., phosphatidylcholine [PC]), and

Figure 4. GLD NPCs display impaired neuronal and glial differentiation

(A–C) Immunofluorescence pictures (A) (d24) and quantification (B and C) (d14 and d24) of cells expressing OLIG2 and APC in UT and LV.hGALC-transduced ND and GLD cultures. Nuclei counterstained with Hoechst (blue). Scale bars, 50 μm.

(D–F) Immunofluorescence pictures (D) (d24) and quantification (E and F) (d14 and d24) of cells expressing TUJ1 (green; neurons) and GFAP (red; astrocytes) in UT and LV.hGALC-transduced ND and GLD neural cultures. Nuclei counterstained with Hoechst (blue). Scale bars, 50 μm.

Data in (B, C, E, and F) are expressed as the percentage of immunoreactive (IR) cells on total nuclei and represent the mean + SEM; n = 2–4 independent experiments/clone/time point; 1–3 clones/group; 5–10 fields/coverslip. Clones used: ND1.2, ND2.1, ND2.2, GLD1.1, GLD1.3, GLD5.2, GLD5.6, ND2.2^{GALC}, GLD1.1^{GALC}, GLD5.2^{GALC}, and GLD5.6^{GALC}. Two-way ANOVA followed by Dunnett's multiple comparison post-test (ND at the corresponding time points selected as control group). *p < 0.05, **p < 0.01, ***p < 0.001.

See also Figures S4 and S5.

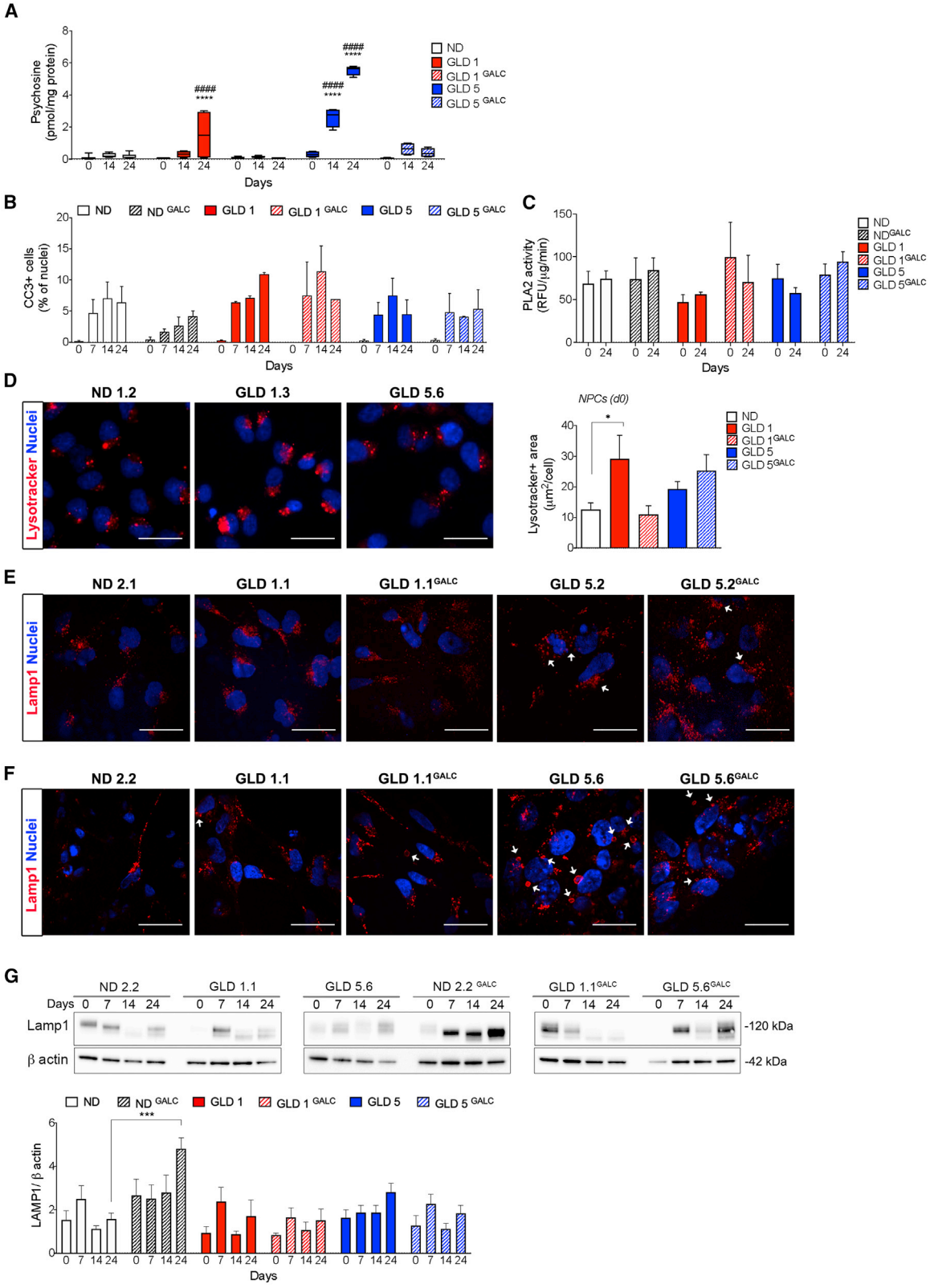

(legend on next page)

differentiated progeny (e.g., phosphatidylethanolamine [PE]; sphingomyelin [SM]) (Figure 7A). We observed profound changes in several phospholipid classes in GLD as compared with ND cells (i.e., TAGs; diacylglycerols [DAG]; monoacylglycerols; PC; PE; lysophosphatidylethanolamine [LPE]; PS; SM; ceramides [Cer]; hexosylceramides [HexCer]) (Figure 7B). Within the same lipid class, we detected differences related to the stage of differentiation (iPSCs versus NPCs versus differentiated cells) and genotype (ND versus GLD1 versus GLD5). The most striking differences between GLD1 and ND cells were observed in NPCs, which showed decreased levels of PE/LPE and increased Cer and DAG levels. When compared with GLD1 and ND cells, GLD5 cells showed reduced PC, PE, HexCer, and SM, and a strong accumulation of DAG, TAG, Cer, and PS (Figure 7B).

LV-mediated rescue of GALC activity partially normalized the lipidomic profiles of GLD1 and GLD5 cells, as shown by principal-component analysis (Figure 7C) and lipid signature (Figures S7A and S7B). In GLD1^{GALC} cells we observed a rescue of PC, PE, HexCer (iPSCs), and TAG (NPCs). In GLD5 ^{GALC} cells we observed the normalization of HexCer and SM level, as well as a normalization of DAG, TAG, and PC. LV-mediated GALC overexpression globally impacted on the lipidome of ND cells. Coherently with the presence of supranormal GALC activity, ND^{GALC} iPSCs, NPCs, and differentiated cells showed decreased levels of HexCer and variable increase of Cer, DAG, and PS in comparison with ND counterparts (Figure S7C).

DISCUSSION

Human iPSCs have been used to model the neural defects associated with several LSDs (Huang et al., 2012; Kobolák et al., 2019). To our knowledge, this is the first report describing a human iPSC-based neural model of GLD. We show that GALC deficiency severely affects the differentiation of human iPSC-derived NPCs into neurons and oligodendrocytes. We highlight cell-type- and patient-specific disease hallmarks in GLD cells, including psychosine storage, lipidome perturbation, and activation of a senescence program. Finally, we show that a timely regulated GALC expression is critical for proper neural commitment and differentiation.

GALC-deficient GLD iPSC lines displayed normal phenotypic and functional properties despite having significant psychosine storage, suggesting the dispensability of the GALC enzyme for somatic cell reprogramming/iPSC maintenance as well as the tolerability to lipid load (Frati et al., 2018). The LV-mediated supply of physiological or slightly supraphysiological GALC activity (3- to 5-fold the ND levels) normalized psychosine levels in GLD iPSCs without affecting their proliferation and neural commitment. The GALC enzyme contributes to preserving the functionality of murine and human HSPCs (Ungari et al., 2015; Visigalli et al., 2010) and murine NPCs (Santambrogio et al., 2012). However, the impact of GALC deficiency and/or overexpression was not investigated in human neural cells. GalCer is a major component of myelin and GALC deficiency primarily

Figure 5. Pathological hallmarks in GLD neural progeny

(A) Psychosine levels (mean + SEM) in UT and LV.hGALC-transduced ND and GLD NPCs (d0) and differentiated progeny (d14 and d24). n = 2–4 independent experiments/clone, 1–3 clones/group. Clones used: ND1.2, ND2.1, ND2.2, GLD1.1, GLD1.3, GLD5.2, GLD5.6, ND2.2^{GALC}, GLD1.1^{GALC}, GLD5.2^{GALC}, and GLD5.6^{GALC}. Two-way ANOVA followed by Tukey's multiple comparison post-test; ****$p < 0.0001$ GLD versus ND at the corresponding time point; ####$p < 0.0001$ GLD versus GLD^{GALC} at the corresponding time point; $p > 0.05$ GLD^{GALC} versus ND at all time points.

(B) Expression of cleaved caspase-3 (CC3) in UT and LV.hGALC-transduced ND and GLD NPCs (d0) and differentiated progeny (d14 and d24). Data (mean + SEM) are expressed as the percentage of immunoreactive cells on total nuclei; n = 2 independent experiments/clone/time point; 1–3 clones/group; 5–10 fields/coverslip. Clones used: ND1.2, ND2.1, ND2.2, GLD1.1, GLD1.3, GLD5.2, GLD5.6, ND2.2^{GALC}, GLD1.1^{GALC}, GLD5.2^{GALC}, and GLD5.6^{GALC}. Two-way ANOVA followed by Dunnett's multiple comparison post-test (ND at the corresponding time point selected as control group). No differences between groups ($p > 0.05$).

(C) PLA2 activity (mean + SEM) in UT and LV.hGALC-transduced ND and GLD NPCs (d0) and differentiated progeny (d24). n = 2 independent experiments; 1–3 clones/group. Clones used: ND1.2, ND2.1, ND2.2, GLD1.1, GLD1.3, GLD5.2, GLD5.6, ND2.2^{GALC}, GLD1.1^{GALC}, GLD5.2^{GALC}, and GLD5.6^{GALC}.

(D) Lysotracker+ NPCs (red) and quantification of Lysotracker+ area (μm^2/cell) in ND1.2, GLD1.3, and GLD5.6 clones. Nuclei counterstained with Hoechst. Scale bars, 15 μm. Data are the mean + SEM, n = 2 independent experiments, 3 wells/clone, 1,400–12,000 cells/well. Two-way ANOVA followed by Dunnett's multiple comparison post-test (ND, control group). *$p < 0.05$.

(E and F) Representative confocal immunofluorescence pictures of LAMP1+ cells (red) at d0 (NPCs; E) and d14 (F) of differentiation. Nuclei counterstained with Hoechst. White arrows indicate enlarged lysosomes. Scale bars, 15 μm.

(G) Western blot and densitometric quantification showing LAMP1 expression in UT and LV.hGALC-transduced ND and GLD NPCs (d0) and differentiated progeny (d7, d14, and d24). β-Actin, loading control. Data are the mean + SEM; n = 3–5 independent experiments; 1–4 clones/group. Two-way ANOVA followed by Dunnett's multiple comparison post-test (ND at the corresponding time point selected as control group). *$p < 0.05$, **$p < 0.01$, ***$p < 0.001$.

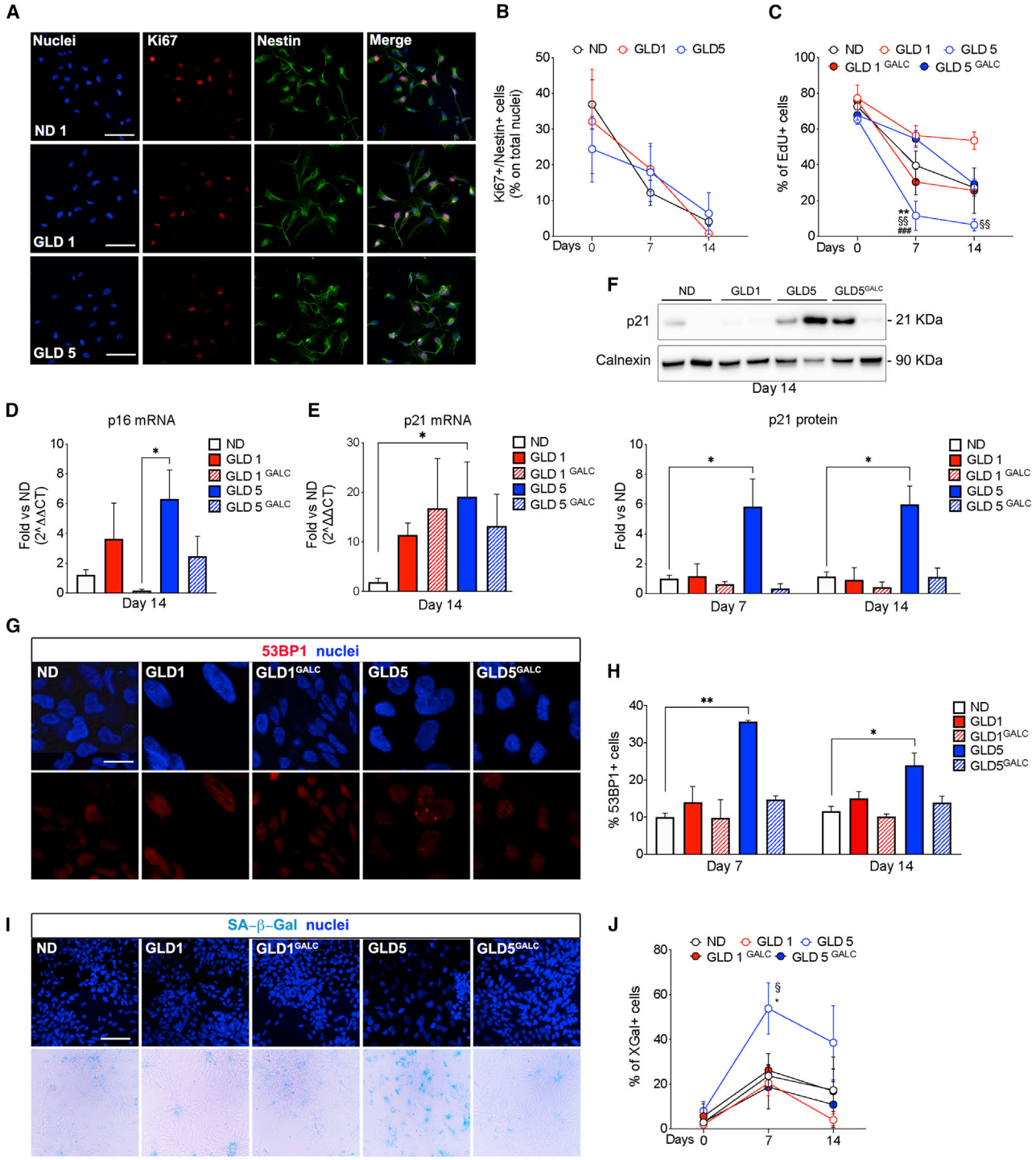

Figure 6. GLD5 NPCs progeny display markers of senescence

(A and B) Immunofluorescence pictures (A) (d0) and quantification (B) (d0, d7) of cells expressing Nestin (green) and Ki67 (red) in ND, GLD, and GLD^{GALC} cultures. Nuclei counterstained with Hoechst. Scale bars, 50 μm. Data are the mean + SEM; n = 3 independent experiments/clone/time point; 1–3 clones/group; 5–10 fields/coverslip were analyzed. Clones used: ND1.2, ND1.3, ND2.1, ND2.2, GLD1.1, GLD1.3, GLD5.2, and GLD5.6.

(C) Quantification of EdU+ cells (after a 16-h pulse) in ND, GLD, and GLD^{GALC} NPCs (d0) and differentiated cultures (d7, d14). Data are expressed as the percentage on total cells (mean + SEM); n = 5 independent experiments, 1–4 clones/group. Clones used: ND1.2, ND2.2,

(legend continued on next page)

affects oligodendroglial development/maturation. Still, the key role of GALC documented in neurons and astrocytes (Misslin et al., 2017; Teixeira et al., 2014) prompted us to model GLD using mixed neuronal/glial cultures. Our NPC-derived ND cultures contained a modest amount of oligodendroglial cells while neurons were more represented. Still, the early (between d7 and d14 of culture) and drastic reduction of oligodendrocytes (observed in all GLD cultures) and neurons (in GLD5 but not GLD1) proved the robustness of the system to highlight early cell loss/defective differentiation that may contribute to neurodevelopmental defects in an early infantile disease. The aggravated time-dependent defects observed in GLD NPC-derived neuronal/glial cultures are in line with the pathological cascades and phenotypes associated with progressive accumulation of psychosine in CNS cells and tissues (Bongarzone et al., 2016; Ricca and Gritti, 2016). Still, several findings in this study suggest a composite- and mutation-dependent effect associated to GALC deficiency besides psychosine toxicity: (1) psychosine accumulation increases along neural differentiation without significant apoptosis; (2) high percentages of marker-negative cells and altered expression of key developmental genes are found in GLD cultures, suggesting a block in cell commitment or differentiation; (3) clearance of psychosine storage in LV.hGALC-transduced GLD neurons/glia partially rescues the differentiation program, with an amelioration in the neuronal compartment but far less improvement in oligodendrocytes.

Many sphingolipids involved in the GALC pathway (e.g., Cer, sphingosine, sphingosine-1-phosphate) contribute to cell proliferation, migration, apoptosis (Hannun and Obeid, 2017), senescence, and autophagy (Trayssac et al., 2018; Young and Wang, 2018). We previously documented the unbalance of some bioactive lipids in murine GLD brain tissues (Santambrogio et al., 2012). Here, we show a distinctive global lipid profile in iPSCs versus NPCs versus NPC progeny, regardless of the genotype (ND, GLD) or mutation (GLD1, GLD5), providing for the first time a snapshot of the changes in lipid metabolism during the iPSC to neural differentiation. Intriguingly, GLD1 and GLD5 cell populations displayed remarkable differences in their lipidomic profile. The accumulation in of TAG, DAG, and Cer in GLD5 iPSCs and NPC progeny may contribute to the early and specific senescence response and differentiation defects observed in these cells, given the role of these lipid species in cell fate, cellular stress, aging, and replicative senescence (Hannun and Obeid, 2017; Lizardo et al., 2017; Venable et al., 1995). Ceramide is the product of GalCer degradation by GALC and its accumulation in GLD5 lines may appear counterintuitive. We speculate that other major pathways leading to Cer production may be induced, i.e., activation of sphingomyelinases and/or Cer synthases (Claus et al., 2009; Mullen et al., 2012). The mechanistic link between the GLD5 mutation and the specific lipid unbalance may include a direct effect of the mutated GALC protein on the lipidome or an indirect effect of another GLD-associated pathology (i.e., oxidative stress, mitochondrial dysfunction) (Ballabio and Gieselmann, 2009). The high vulnerability of neurons to these stressful

GLD1.1, GLD5.2, GLD5.4, GLD5.5, GLD5.6, GLD1.1^{GALC}, GLD5.2^{GALC}, and GLD5.6^{GALC}. Two-way ANOVA followed by Tukey's multiple comparison post-test, **p < 0.01 GLD5 versus ND at d7; §§p < 0.01 GLD5 versus GLD1 at d7 and d14; ###p < 0.001 GLD5 versus GLD5^{GALC} at d7; p > 0.05 GLD5^{GALC} versus ND and GLD1 versus ND at all time points.

(D and E) Expression of p16 (*CDKN2A*; D) and p21 (*CDKN1A*; E) mRNA in ND, GLD, and GLD^{GALC} cultures (d14). n = 5 independent experiments/clone; 1–4 clones/group. Clones used: ND1.2, ND2.2, GLD1.1, GLD1.3, GLD5.2, GLD5.4, GLD5.5, GLD5.6, GLD1.1^{GALC}, GLD5.2^{GALC}, and GLD5.6^{GALC}. Data (mean + SEM) are normalized on the housekeeping gene β-glucuronidase (*GUSB*) and expressed as fold change ($2^{-\Delta\Delta CT}$) versus ND (mean of all samples). Kruskal-Wallis test followed by Dunn's multiple comparison post-test; *p < 0.05.

(F) Western blot and densitometric quantification showing the expression of the p21 protein in ND, GLD, and GLD^{GALC} differentiated cultures at d7 and d14 (shown in the blot). Calnexin, loading control. Data are expressed as fold versus ND at the corresponding time point (mean of all clones) and plotted as the mean + SEM; n = 4 independent experiments; 1–4 clones/group. Clones used: ND1.2, ND2.2, GLD1.1, GLD1.3, GLD5.2, GLD5.4, GLD5.5, GLD5.6, GLD1.1^{GALC}, GLD5.2^{GALC}, and GLD5.6^{GALC}. Two-way ANOVA followed by Dunnett's multiple comparison post-test (ND at the corresponding time point selected as control group); *p < 0.05.

(G and H) Confocal immunofluorescence pictures (G) and quantification (H) of 53BP1+ DDR foci in ND, GLD, and GLD^{GALC} NPCs (d0) and differentiated cultures at d7 and d14 (shown in the pictures). Nuclei counterstained with DAPI. Scale bars, 15 μm (all panels, shown in ND). Clones used: ND1.2, ND2.2, GLD1.1, GLD1.3, GLD5.2, GLD5.6, GLD1.1^{GALC}, GLD5.2^{GALC}, and GLD5.6^{GALC}. Data are the mean + SEM; n = 3 independent experiments/clone/time point; 100–600 nuclei/group. Kruskal-Wallis test followed by Dunn's multiple comparison post-test (ND at the corresponding time points selected as control group); *p < 0.05, **p < 0.01.

(I and J) Representative pictures (I) (bright-field and Hoechst fluorescence for nuclei) and quantification (J) of SA-βGAL+ cells in ND, GLD, and GLD^{GALC} NPCs (d0) and differentiated cultures at d7 (shown in the pictures) and d14. Scale bars, 50 μm (all panels, shown in ND). Data are the mean + SEM n = 3 independent experiments/clone/time point; 1–3 clones/group; 4–10 fields/coverslip. Clones used: ND1.2, ND2.1, ND2.2, GLD1.1, GLD5.2, GLD5.6, GLD1.1^{GALC}, GLD5.2^{GALC}, and GLD5.6^{GALC}. Two-way ANOVA followed by Tukey's multiple comparison post-test; *p < 0.05 GLD5 versus ND at d7; §p < 0.05 GLD5 versus GLD1 at d7; p > 0.05 GLD5^{GALC} versus ND and GLD1 versus ND at all time points. See also Figure S6.

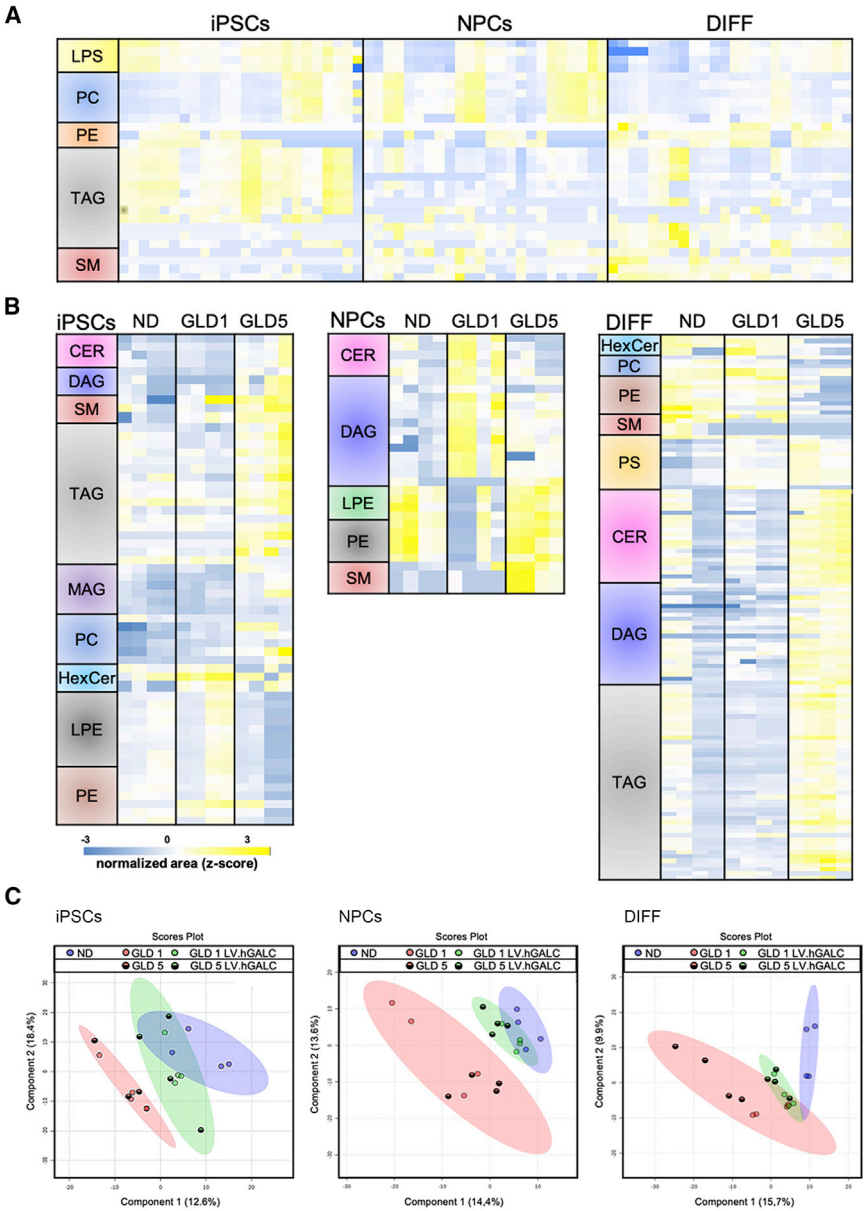

Figure 7. Lipidomic profile during iPSC neural differentiation

(A) Hierarchical clustering of lipid species differently enriched in iPSCs, NPCs, and differentiated cultures (d14). ANOVA statistical test was applied (false discovery rate [FDR] < 0.05).

(B) Hierarchical clustering of lipid species differently enriched in ND, GLD1 and GLD5 iPSCs, NPCs and differentiated cultures (d14). ANOVA statistical test was applied (FDR < 0.05).

(C) Principal-component analysis (PCA) of lipid species distribution in ND, GLD and LV.hGALC-transduced GLD iPSCs, NPCs, and differentiated cultures (d14 of differentiation). Clones used: ND2.2, GLD1.1, GLD5.2, ND2.2^{GALC}, GLD1.1^{GALC}, and GLD5.2^{GALC}. See supplemental experimental procedures for abbreviations of lipid classes.

See also Figure S7.

events would explain the dramatic neuronal phenotype observed in GLD5 clones. The use of isogenic pairs might clarify whether the GLD5 mutated protein has a dominant-negative effect that contributes to the pathogenic phenotype in addition to the enzymatic deficiency. Also, the respective role and potential interaction between psychosine load and lipidome perturbation are not fully elucidated but could involve a detrimental action of psychosine (accumulated in both GLD5 and GLD1 cells) and Cer (and other lipid classes, e.g., TAG; accumulated in GLD5) preferentially on oligodendrocyte and neuronal cells, respectively (Jana et al., 2009). The little residual psychosine storage in LV.hGALC-transduced GLD5 cells may account for the incomplete rescue of both oligodendrocytes and neurons. The lipidomic profile is overall normalized in LV.hGALC-transduced GLD5 cells but we cannot exclude harmful effects due to a minor lipid unbalance.

The association between lysosomal dysfunction, lipid unbalance, and senescence in NPCs, neurons, and glial cells, and its contribution to neurodegeneration and demyelination is emerging as an area of active scientific investigations. Specifically, by taking advantage of mouse models or postmortem human brain samples it was reported that senescence functionally contributes to multiple sclerosis

pathogenesis (Nicaise et al., 2019) as well as to cognitive defects in Alzheimer disease (Zhang et al., 2019). Notably, our study highlights the importance of performing this investigation in relevant human iPSC-based neural models, which recapitulate the patient-specific pathological hallmarks more faithfully as compared with murine models or non-neural cells. These findings represent a starting point for future functional experiments aimed at further dissecting the complex and mutation-specific GLD pathology. This knowledge will pave the way to tailored gene/cell therapy strategies to enhance the correction of CNS pathology in GLD.

EXPERIMENTAL PROCEDURES

Reprogramming of human fibroblasts and generation of hiPSCs

Human dermal fibroblasts from healthy donors (ND1 and ND2) were purchased from Life Technologies. Fibroblasts from GLD patients (GLD1, GLD2, GLD3, GLD4, and GLD5) and of a non-affected relative of GLD1 (ND3) were obtained from the Cell Line and DNA Bank of Patients affected by Genetic Diseases (Gaslini Institute, Genova, Italy). Human fibroblasts were cultured in Dulbecco's modified Eagle's medium supplemented with 10% fetal bovine serum, L-glutamine, and penicillin/streptomycin in a humidified atmosphere, 5% CO_2 at 37°C. Fibroblasts at passages (p) 4–5 (GLD1, GLD2, GLD3, ND1, ND2) and p10–11 (GLD4 and GLD5, ND3) were used for reprogramming. The StemMACS mRNA Reprogramming Kit (Miltenyi Biotec, Bergisch Gladbach, Germany) was used for mRNA transfection according to the manufacturer's instructions. See the supplemental experimental procedures for details on iPSC culture, expansion, karyotype analysis, and embryoid body formation.

iPSC differentiation into NPCs and mixed neuronal/glial cultures

We applied a published protocol (Chambers et al., 2009) for neural induction of iPSCs. The newly generated NPCs could be expanded for four to six passages. We differentiated NPCs (passages 2–3) using a published protocol (Frati et al., 2018) with some modifications. Details can be found in the supplemental experimental procedures.

Lentiviral vector-mediated *hGALC* gene transfer in iPSCs

We used a laboratory-grade/scale third-generation LV encoding the human (h)*GALC* cDNA tagged with the myc peptide, under control of the human PGK promoter (Meneghini et al., 2016). Transduced cells were used for the experiments after three to four subculturing passages, when only integrated LV genome is present.

Quantification of psychosine

Psychosine quantification was performed on frozen cell pellets using a TSQ Quantum AM mass spectrometer (Thermo Fisher Scientific, Waltham, USA) as described previously (Lattanzi et al., 2014).

Measurement of GALC activity

Specific GALC activity was measured as described previously (Martino et al., 2009)(Ricca et al., 2015).

Measurement of PLA2 activity

PLA2 activity was measured using the EnzChek Phospholipase A2 Assay Kit (Thermo Fisher), according to the manufacturer's instructions. The enzymatic activity is expressed as relative fluorescent units/μg of protein/min.

SA-β-GAL assay (X-GAL staining) and proliferation analysis (EdU staining)

We used the SA-β-GAL Staining Kit (Cell Signaling Technology, Danvers, USA) following the manufacturer's instructions.

We assessed cell proliferation using EdU, supplied with Click-iT EdU Alexa Fluor 647 Imaging Kit (Thermo Fisher Scientific). See the supplemental experimental procedures for more details.

High-throughput live cell microscopy

The lysosomal area was quantified using a high-content imaging platform (ArrayScan XTI HCA Reader, Thermo Fisher Scientific). See the supplemental experimental procedures for more details.

Immunofluorescence analysis

IF analysis was performed as described previously (Frati et al., 2018). See the supplemental experimental procedures for more details. A list of primary and secondary antibodies is found in Table S3.

Western blot analysis

Details on WB blot analysis can be found in the supplemental experimental procedures. A list of primary and secondary antibodies is found in Table S4.

Molecular analysis

Methods for sequencing of patient mutations and gene expression analysis (RT-PCR; SYBR green and TaqMan RT-PCR) are found in the supplemental experimental procedures.

The list of primers used for PCR amplification and sequencing is found in Table S5.

The list of primers and probes used for gene expression analyses is found in Table S6.

Determination of VCN

Genomic DNA was extracted from cell pellets using a Maxwell Cell DNA Purification Kit (Promega) or a QIAamp DNA Micro Kit (QIAGEN), depending on the number of cells. The number of integrated vector copies/genome was quantified by TaqMan analysis, as described previously (Lattanzi et al., 2014). See the supplemental experimental procedures for more details.

Lipidomic analyses

Details on lipid extraction, protein quantification, lipid profiling data acquisition, processing, and analysis can be found in the supplemental experimental procedures.

Statistics

Data were analyzed with GraphPad Prism version 8 for Macintosh and expressed as the mean ± standard error of the mean (SEM). The number of samples and the statistical tests and post-tests used are specified in the legends to each figure. $p < 0.05$ was considered statistically significant.

For lipid analyses, statistical analysis was performed using Metaboanalyst 4.0 web tool https://www.metaboanalyst.ca/MetaboAnalyst/faces/home.xhtml.

Data and code availability

Reagents generated in this study are available upon request from the lead contact with a completed MTA.

The lipidomic dataset reported in this paper is available at MetaboLights, accession number MTBLS1501 (https://www.ebi.ac.uk/metabolights/MTBLS1501).

SUPPLEMENTAL INFORMATION

Supplemental information can be found online at https://doi.org/10.1016/j.stemcr.2021.04.011.

AUTHOR CONTRIBUTIONS

Conceptualization, A.G. and E.M.; methodology, E.M., A.B., R.D.M., and S.M.; investigation, E.M., A. Cecchele, A. Cattaneo, F.M., D.G., L.d.V., V.M., F.S., M.P, and L.S.; writing – review & editing, A.G., E.M., R.D.M., and A.B.; funding acquisition, A.G.; resources, S.M., A.B., R.D.M., and F.S.; supervision, A.G., R.D.M., and A.B.

ACKNOWLEDGMENTS

We are grateful to Lucia Sergi Sergi for LV preparation and titration, Andrea Ditadi for providing the ESC line H9, Wim Kulik for psychosine analyses, Janet E. Deane for providing the anti-hGALC antibody, all the members of the Gritti's lab for generous support and helpful discussion. Part of this work was carried out in ALEMBIC, an advanced microscopy laboratory established by IRCCS Ospedale San Raffaele and Università Vita-Salute San Raffaele. We thank the "Diagnosi PrePostnatale Malattie Metaboliche" Laboratory (G. Gaslini Institute) for providing us with specimens from the "Cell line and DNA bank from patients affected by Genetic diseases" Biobank—Telethon Genetic Biobank Network (project no. GTB07001A). This study was funded by grants from Fondazione Telethon (Tiget Core Grant 2016-2021, grantD2), European Leukodystrophy Association (grant ELA 2016-010I3), European Joint Program on Rare Diseases (EJP RD; project NG4Leuko) to A.G. R.D.M. was supported by Fondazione Telethon (Tiget Core Grant 2016-2021, grant E5), a Career Development Award from Human Frontier Science Program (HFSP), an Advanced Research Grant from the European Hematology Association (EHA), "Pilot and Seed Grant 2015" from the San Raffaele Hospital, a Hollis Brownstein Research Grant from Leukemia Research Foundation (LRF), the Interstellar Initiative on Healthy Longevity from NYAS and AMED, and by AIRC (MFAG 2019 - ID. 23321 project). R.D.M. is a New York Stem Cell Foundation Robertson Investigator. D.G. was supported by the IBSA Foundation postdoctoral fellowship. E.M. was supported by an FCSR (Fondazione Centro San Raffaele) postdoctoral fellowship. E.M., A. Cecchele, and L.d.V. conducted this study as partial fulfillment of their international Ph.D. in Molecular Medicine, Vita-Salute San Raffaele University.

Received: August 26, 2020
Revised: April 15, 2021
Accepted: April 16, 2021
Published: May 13, 2021

REFERENCES

Allewelt, H.B., Page, K., Taskindoust, M., Troy, J.D., Wood, S., Parikh, S., Prasad, V.K., and Kurtzberg, J. (2016). Long-term functional outcomes following hematopoietic stem cell transplantation for Krabbe disease. Biol. Blood Marrow Transpl. *22*, S102–S103.

Ballabio, A., and Gieselmann, V. (2009). Lysosomal disorders: from storage to cellular damage. Biochim. Biophys. Acta *1793*, 684–696.

Bongarzone, E.R., Escolar, M.L., Gray, S.J., Kafri, T., Vite, C.H., and Sands, M.S. (2016). Insights into the pathogenesis and treatment of Krabbe disease. Pediatr. Endocrinol. Rev. *13*, 689–696.

Bradbury, A.M., Bongarzone, E.R., and Sands, M.S. (2021). Krabbe disease: new hope for an old disease. Neurosci. Lett. *752*, 135841.

Chambers, S.M., Fasano, C.A., Papapetrou, E.P., Tomishima, M., Sadelain, M., and Studer, L. (2009). Highly efficient neural conversion of human ES and iPS cells by dual inhibition of SMAD signaling. Nat. Biotechnol. *27*, 275–280.

Claus, R., Dorer, M., Bunck, A., and Deigner, H. (2009). Inhibition of sphingomyelin hydrolysis: targeting the lipid mediator ceramide as a key regulator of cellular fate. Curr. Med. Chem. *16*, 1978–2000.

De Gasperi, R., Gama Sosa, M.A., Sartorato, E., Battistini, S., Raghavan, S., and Kolodny, E.H. (1999). Molecular basis of late-life globoid cell leukodystrophy. Hum. Mutat. *14*, 256–262.

Del Grosso, A., Angella, L., Tonazzini, I., Moscardini, A., Giordano, N., Caleo, M., Rocchiccioli, S., and Cecchini, M. (2019). Dysregulated autophagy as a new aspect of the molecular pathogenesis of Krabbe disease. Neurobiol. Dis. *129*, 195–207.

Folts, C.J., Scott-Hewitt, N., Pröschel, C., Mayer-Pröschel, M., and Noble, M. (2016). Lysosomal re-acidification prevents lysosphingolipid-induced lysosomal impairment and cellular toxicity. PLoS Biol. *14*, e1002583.

Frati, G., Luciani, M., Meneghini, V., De Cicco, S., Ståhlman, M., Blomqvist, M., Grossi, S., Filocamo, M., Morena, F., Menegon, A., et al. (2018). Human iPSC-based models highlight defective glial and neuronal differentiation from neural progenitor cells in metachromatic leukodystrophy. Cell Death Dis. *9*, 698.

Hannun, Y.A., and Obeid, L.M. (2017). Sphingolipids and their metabolism in physiology and disease. Nat. Rev. Mol. Cell Biol. *19*, 175–191.

He, S., and Sharpless, N.E. (2017). Senescence in health and disease. Cell *169*, 1000–1011.

Huang, H.-P., Chuang, C.-Y., and Kuo, H.-C. (2012). Induced pluripotent stem cell technology for disease modeling and drug screening with emphasis on lysosomal storage diseases. Stem Cell Res. Ther. *3*, 34.

Irahara-Miyana, K., Otomo, T., Kondo, H., Hossain, M.A., Ozono, K., and Sakai, N. (2018). Unfolded protein response is activated in Krabbe disease in a manner dependent on the mutation type. J. Hum. Genet. *63*, 699–706.

Jalal, K., Carter, R., Yan, L., Barczykowski, A., and Duffner, P.K. (2012). Does galactocerebrosidase activity predict Krabbe phenotype? Pediatr. Neurol. *47*, 324–329.

Jana, A., Hogan, E.L., and Pahan, K. (2009). Ceramide and neurodegeneration: susceptibility of neurons and oligodendrocytes to cell damage and death. J. Neurol. Sci. *278*, 5–15.

Jatana, M., Giri, S., and Singh, A.K. (2002). Apoptotic positive cells in Krabbe brain and induction of apoptosis in rat C6 glial cells by psychosine. Neurosci. Lett. *330*, 183–187.

Kobolák, J., Molnár, K., Varga, E., Bock, I., Jezsó, B., Téglási, A., Zhou, S., Lo Giudice, M., Hoogeveen-Westerveld, M., Pijnappel, W.P., et al. (2019). Modeling the neuropathology of lysosomal storage disorders through disease-specific human induced pluripotent stem cells. Exp. Cell Res. *380*, 216–233.

Lattanzi, A., Salvagno, C., Maderna, C., Benedicenti, F., Morena, F., Kulik, W., Naldini, L., Montini, E., Martino, S., and Gritti, A. (2014). Therapeutic benefit of lentiviral-mediated neonatal intracerebral gene therapy in a mouse model of globoid cell leukodystrophy. Hum. Mol. Genet. *23*, 3250–3268.

Lee, W.C., Kang, D., Causevic, E., Herdt, A.R., Eckman, E.A., and Eckman, C.B. (2010). Molecular characterization of mutations that cause globoid cell leukodystrophy and pharmacological rescue using small molecule chemical chaperones. J. Neurosci. *30*, 5489–5497.

Lizardo, D.Y., Lin, Y.L., Gokcumen, O., and Atilla-Gokcumen, G.E. (2017). Regulation of lipids is central to replicative senescence. Mol. Biosyst. *13*, 498–509.

Luzi, P., Rafi, M.A., and Wenger, D.A. (1995). Characterization of the large deletion in the GALC gene found in patients with Krabbe disease. Hum. Mol. Genet. *4*, 2335–2338.

Martino, S., Tiribuzi, R., Tortori, A., Conti, D., Visigalli, I., Lattanzi, A., Biffi, A., Gritti, A., and Orlacchio, A. (2009). Specific determination of beta-galactocerebrosidase activity via competitive inhibition of beta-galactosidase. Clin. Chem. *55*, 541–548.

Meneghini, V., Lattanzi, A., Tiradani, L., Bravo, G., Morena, F., Sanvito, F., Calabria, A., Bringas, J., Fisher-Perkins, J.M., Dufour, J.P., et al. (2016). Pervasive supply of therapeutic lysosomal enzymes in the CNS of normal and Krabbe-affected non-human primates by intracerebral lentiviral gene therapy. EMBO Mol. Med. *8*, 489–510.

Misslin, C., Velasco-Estevez, M., Albert, M., O'Sullivan, S.A., and Dev, K.K. (2017). Phospholipase A2 is involved in galactosylsphingosine-induced astrocyte toxicity, neuronal damage and demyelination. PLoS One *12*, e0187217.

Mullen, T.D., Hannun, Y.A., Obeid, L.M., Hannun, Y.A., Obeid, L.M., Gatt, S., Gatt, S., Yavin, E., Gatt, S., Sribney, M., et al. (2012). Ceramide synthases at the centre of sphingolipid metabolism and biology. Biochem. J. *441*, 139–150.

Nicaise, A.M., Wagstaff, L.J., Willis, C.M., Paisie, C., Chandok, H., Robson, P., Fossati, V., Williams, A., and Crocker, S.J. (2019). Cellular senescence in progenitor cells contributes to diminished remyelination potential in progressive multiple sclerosis. Proc. Natl. Acad. Sci. U S A *116*, 9030–9039.

Orsini, J.J., Escolar, M.L., Wasserstein, M.P., and Caggana, M. (2000). Krabbe disease. Jun 19 [updated 2018 Oct 11]. In GeneReviews® [Internet], M.P. Adam, H.H. Ardinger, R.A. Pagon, S.E. Wallace, L.J.H. Bean, K. Stephens, and A. Amemiya, eds. (University of Washington, Seattle), pp. 1993–2021.

Pellegrini, D., Del Grosso, A., Angella, L., Giordano, N., Dilillo, M., Tonazzini, I., Caleo, M., Cecchini, M., and McDonnell, L.A. (2019). Quantitative microproteomics based characterization of the central and peripheral nervous system of a mouse model of Krabbe disease. Mol. Cell. Proteomics *8*, 1227–1241.

Ribbens, J., Whiteley, G., Furuya, H., Southall, N., Hu, X., Marugan, J., Ferrer, M., and Maegawa, G.H.B. (2013). A high-throughput screening assay using Krabbe disease patient cells. Anal. Biochem. *434*, 15–25.

Ricca, A., Rufo, N., Ungari, S., Morena, F., Martino, S., Kulik, W., Alberizzi, V., Bolino, A., Bianchi, F., Del Carro, U., et al. (2015). Combined gene/cell therapies provide long-term and pervasive rescue of multiple pathological symptoms in a murine model of globoid cell leukodystrophy. Hum. Mol. Genet. *24*, 3372–3389.

Ricca, A., and Gritti, A. (2016). Perspective on innovative therapies for globoid cell leukodystrophy. J. Neurosci. Res. *94*, 1304–1317.

Santambrogio, S., Ricca, A., Maderna, C., Ieraci, A., Aureli, M., Sonnino, S., Kulik, W., Aimar, P., Bonfanti, L., Martino, S., et al. (2012). The galactocerebrosidase enzyme contributes to maintain a functional neurogenic niche during early post-natal CNS development. Hum. Mol. Genet. *21*, 4732–4750.

Shi, Y., Inoue, H., Wu, J.C., and Yamanaka, S. (2017). Induced pluripotent stem cell technology: a decade of progress. Nat. Rev. Drug Discov. *16*, 115–130.

Shin, D., Feltri, M.L., and Wrabetz, L. (2016). Altered trafficking and processing of GALC mutants correlates with globoid cell leukodystrophy severity. J. Neurosci. *36*, 1858–1870.

Spratley, S.J., Hill, C.H., Viuff, A.H., Edgar, J.R., SkjØdt, K., and Deane, J.E. (2016). Molecular mechanisms of disease pathogenesis differ in Krabbe disease variants. Traffic *17*, 908–922.

Suzuki, K., and Suzuki, Y. (1970). Globoid cell leucodystrophy (Krabbe's disease): deficiency of galactocerebroside beta-galactosidase. Proc. Natl. Acad. Sci. U S A *66*, 302–309.

Teixeira, C.A., Miranda, C.O., Sousa, V.F., Santos, T.E., Malheiro, A.R., Solomon, M., Maegawa, G.H., Brites, P., and Sousa, M.M. (2014). Early axonal loss accompanied by impaired endocytosis, abnormal axonal transport, and decreased microtubule stability occur in the model of Krabbe's disease. Neurobiol. Dis. *66*, 92–103.

Trayssac, M., Hannun, Y.A., and Obeid, L.M. (2018). Role of sphingolipids in senescence: implication in aging and age-related diseases. J. Clin. Invest. *128*, 2702–2712.

Ungari, S., Montepeloso, A., Morena, F., Cocchiarella, F., Recchia, A., Martino, S., Gentner, B., Naldini, L., and Biffi, A. (2015). Design of a regulated lentiviral vector for hematopoietic stem cell gene therapy of globoid cell leukodystrophy. Mol. Ther. Methods Clin. Dev. *2*, 15038.

Venable, M.E., Lee, J.Y., Smyth, M.J., Bielawska, A., and Obeid, L.M. (1995). Role of ceramide in cellular senescence. J. Biol. Chem. *270*, 30701–30708.

Visigalli, I., Ungari, S., Martino, S., Park, H., Cesani, M., Gentner, B., Sergi Sergi, L., Orlacchio, A., Naldini, L., and Biffi, A. (2010). The galactocerebrosidase enzyme contributes to the maintenance of a functional hematopoietic stem cell niche. Blood *116*, 1857–1866.

Wenger, D.A. (2000). Murine, canine and non-human primate models of Krabbe disease. Mol. Med. Today *6*, 449–451.

White, A.B., Galbiati, F., Givogri, M.I., Lopez Rosas, A., Qiu, X., Van Breemen, R., and Bongarzone, E.R. (2011). Persistence of psychosine in brain lipid rafts is a limiting factor in the therapeutic recovery of a mouse model for Krabbe disease. J. Neurosci. Res. *89*, 352–364.

Yamanaka, S. (2007). Strategies and new developments in the generation of patient-specific pluripotent stem cells. Cell Stem Cell *1*, 39–49.

Young, M.M., and Wang, H.G. (2018). Sphingolipids as regulators of autophagy and endocytic trafficking. Adv. Cancer Res. *140*, 27–60.

Zhang, P., Kishimoto, Y., Grammatikakis, I., Gottimukkala, K., Cutler, R.G., Zhang, S., Abdelmohsen, K., Bohr, V.A., Misra Sen, J., Gorospe, M., et al. (2019). Senolytic therapy alleviates Aβ-associated oligodendrocyte progenitor cell senescence and cognitive deficits in an Alzheimer's disease model. Nat. Neurosci. *22*, 719–728.